Chapter 4
Bio-ceramic Coating of Ca–Ti–O System Compound by Laser Chemical Vapor Deposition

Hirokazu Katsui and Takashi Goto

Abstract Bio-ceramic Ca–Ti–O system compound films were prepared by laser chemical vapor deposition (laser CVD). Laser CVD is a high-speed technique for coating films with versatile controllability of microstructures and crystal phases. Highly oriented $CaTiO_3$ films with specific textures and $Ca_{n+1}Ti_nO_{3n+1}$ films with the Ruddlesden–Popper-type structure were prepared at high deposition rates. The formation of calcium phosphate in simulated body fluid (SBF) was promoted by $Ca_{n+1}Ti_nO_{3n+1}$ films.

Keywords Calcium titanate • Laser CVD • Microstructure • Bioactive coating • High deposition rate

4.1 Introduction

Ti and Ti-based alloys are used as artificial bones and dental implants because of their acceptable mechanical properties, low weight, and adequate corrosion resistance in the human body. However, they suffer certain disadvantages, such as poor osteoinductive properties and a duration of several months for the reconstruction of the bone/implant interface with adequate adhesion. The osseointegration of an orthopedic implant involves a cascade of cellular and extracellular biological events that occur at the bone/implant interface [1]. The processes can be enhanced by the surface treatments and bio-ceramic coating on implants [2, 3]. The plasma-sprayed hydroxyapatite ($Ca_{10}(PO_4)_6(OH)_2$, HAp) coating on Ti is practically used for dental implants [3, 4]. However, the low interface bonding strength and coating toughness can cause a fracture in the interface between HAp and Ti implants. HAp films with low crystallinity coated on Ti implants dissolve rapidly when Ti is implanted into a

H. Katsui (✉) • T. Goto
Institute for Materials Research, Tohoku University,
2-1-1 Katahira, Aoba-ku, Sendai, Miyagi 980-8577, Japan
e-mail: katsui@imr.tohoku.ac.jp

K. Sasaki et al. (eds.), *Interface Oral Health Science 2016*,
DOI 10.1007/978-981-10-1560-1_4

human body. The crystallinity and microstructure of coated films is an important factor for establishing a good interface between the bone and implants [4, 5].

Recently, calcium titanate ($CaTiO_3$) has gained considerable attention as a biomaterial. $CaTiO_3$ coatings with controlled thickness and crystallinity are effective for bone formation because $CaTiO_3$ is chemically stable at low pH and can form HAp in SBF [6–8]. $CaTiO_3$ has also been proposed as an intermediate layer to improve the adhesion between HAp and Ti-based implants [9–13]. To date, a variety of techniques, such as sol–gel [13], hydrothermal reactions [14], ion implantation [15], sputtering [8], and anode oxidation techniques [7], were employed for $CaTiO_3$ coating. Chemical vapor deposition (CVD) is a versatile technique to prepare various ceramic films and is widely used in the industry. Sato et al. reported the synthesis of $CaTiO_3$ films by CVD using metal organic precursors followed by apatite formation on the film surface upon immersion in SBF [16]. Auxiliary energies such as plasmas and lasers could be employed to accelerate chemical reactions and prepare highly crystalline films with controlled morphology and crystal phases at high deposition rates [17–21]. In this study, we demonstrate the synthesis of Ca–Ti–O films by laser CVD, and the effects of deposition parameters on crystal phases, morphology, and deposition rate are investigated. Laser CVD can produce $Ca_{n+1}Ti_nO_{3n+1}$ films which exhibited a significant formability of calcium phosphate precipitates on the coating surface in the SBF immersion.

4.2 Laser Chemical Vapor Deposition

CVD is a gas-phase deposition process, comprising several chemical reactions between source gases (precursors). Dense films can be coated by CVD even on rough surfaces with high adherence and good conformal coverage. This is advantageous for bio-ceramic coatings on complex-shaped dental implants and artificial bones. Hence, bio-ceramic coatings of well-crystallized Ca–P–O system compounds, such as HAp, α- and β-$Ca_3P_2O_8$, $Ca_4P_2O_9$, and α- and β-$Ca_2P_2O_7$, have been performed using CVD [22–24]. Generally, the deposition rate of CVD is lower than that of plasma spray and electron beam physical vapor deposition. In conventional thermal CVD, the chemical reaction at the interface between the gas and substrate surface is driven by thermal energy. Laser irradiation can accelerate the chemical reactions and enable low-temperature deposition to avoid degradation and corrosion of the substrate materials. Figure 4.1 shows a schematic of the laser CVD apparatus for the coating of Ca–Ti–O compounds. The source materials (precursors) of Ca and Ti were evaporated, and the source vapors were introduced into a CVD reaction chamber. Oxygen was separately introduced into the chamber. A substrate was placed on a hot stage for preheating. The substrate surface was irradiated by an Nd:YAG laser (wavelength 1064 nm) through a quartz window. By controlling deposition parameters, such as laser power, deposition temperature, total pressure, and precursor supply conditions, various forms of deposits can be obtained, e.g., amorphous, fine crystals, columnar crystals, dendritic crystals, whiskers, plate-like

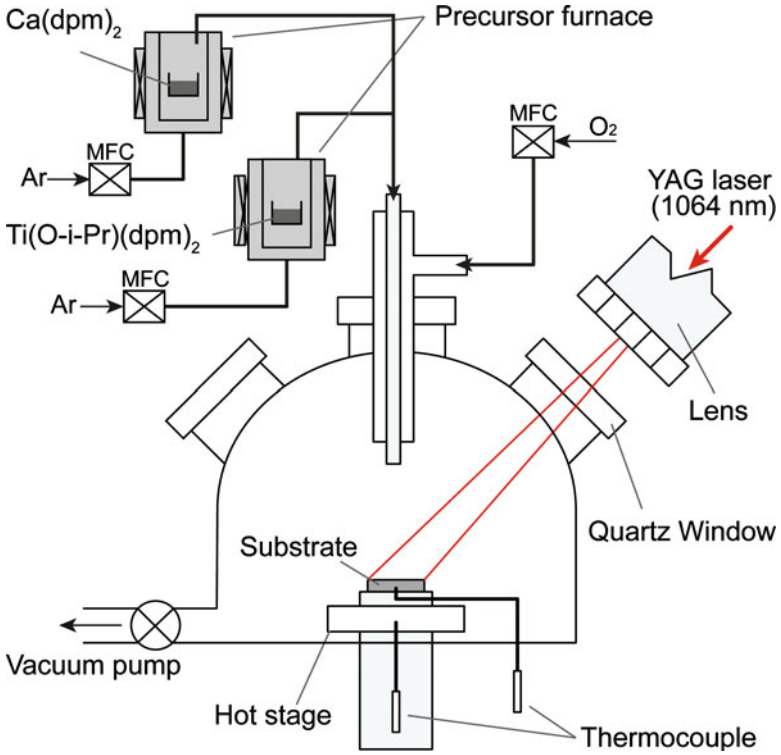

Fig. 4.1 Schematic of laser CVD apparatus

crystals, and epitaxial single-crystal films. In this study, aluminum nitride (AlN) was first used as the substrate, because it is thermochemically stable at high temperature, and its good workability enables us to investigate the effect of a wide range of CVD parameters on the Ca–Ti–O film characteristics. Based on the insight into the correlation between the CVD parameters and the film characteristics using the AlN substrates, bioactive Ca–Ti–O films were coated on metallic Ti substrates under optimum laser CVD conditions.

4.3 Bio-ceramic Coating of Ca–Ti–O by Laser CVD [25, 26]

The phase diagram of a $CaO–TiO_2$ pseudo-binary system is shown in Fig. 4.2 [27, 28]. At a Ca/Ti ratio of 1.0, the $CaTiO_3$ phase exists, which is the most common calcium titanate compound. No other phases are stable in the Ti-rich region between TiO_2 and $CaTiO_3$, whereas $Ca_{n+1}Ti_nO_{3n+1}$ phases exist in the Ca-rich region between $CaTiO_3$ and CaO. The crystal structures of $CaTiO_3$ and $Ca_{n+1}Ti_nO_{3n+1}$ are illustrated in Fig. 4.3. Further $CaTiO_3$ has a perovskite structure with a space group of *Pnma*,

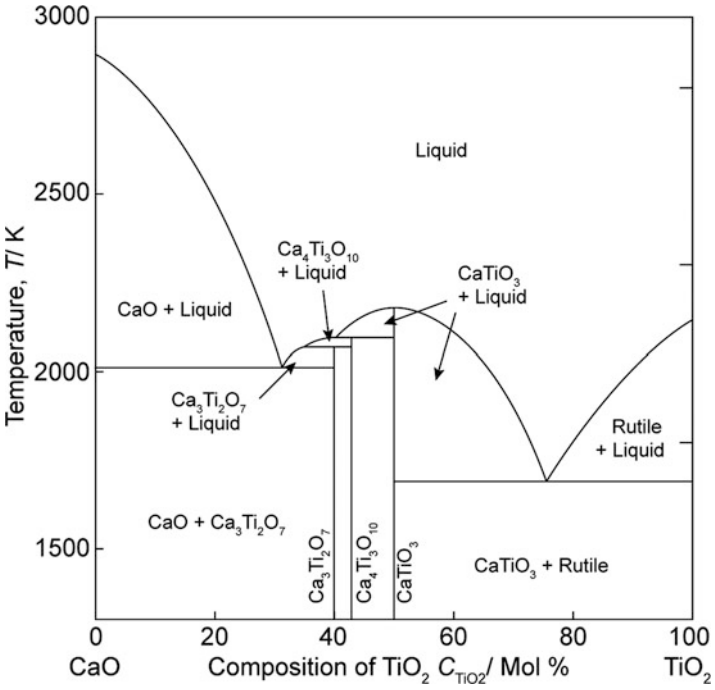

Fig. 4.2 Phase diagram of CaO–TiO_2 system [27, 28]

comprising the corner-sharing TiO_6 octahedra surrounded by Ca ions with a 12-fold coordination [29]. The $Ca_{n+1}Ti_nO_{3n+1}$ phases have perovskite-related structures, the so-called Ruddlesden–Popper structure, formed by alternate stacking of perovskite blocks and CaO layers, as shown in Fig. 4.3 [30]. The stacking sequence in a unit cell corresponds to the n value in $Ca_{n+1}Ti_nO_{3n+1}$. Two phases, $Ca_2Ti_3O_7$ ($n=2$) and $Ca_3Ti_4O_{10}$ ($n=3$), have been reported to exist in the TiO_2–CaO system. Although $CaTiO_3$ films fabricated by various methods and their bioactivities were investigated using in vivo and in vitro experiments [3, 6, 8, 10, 11, 13], there are few reports of the synthesis of $Ca_{n+1}Ti_nO_{3n+1}$ films as a biomaterial [31]. Laser CVD can be used to synthesize $CaTiO_3$ and $Ca_{n+1}Ti_nO_{3n+1}$ by controlling deposition parameters, such as the Ca/Ti supply ratio of the precursors and deposition temperature depending on the laser power. Figure 4.4 depicts the effects of deposition temperature and Ca/Ti supply ratio on the phase formation of Ca–Ti–O films by laser CVD. At a Ca/Ti supply ratio of approximately 1.0, single-phase $CaTiO_3$ films were formed at deposition temperatures below 1100 K. At deposition temperatures above 1100 K, $CaTiO_3$ films contained TiO_2, Ca–Al–O compounds (e.g., $CaAl_2O_4$ and $CaAl_4O_7$) and Al_2O_3, resulting in a reaction between the source gases and the AlN substrate at high temperatures. At Ca/Ti supply ratios <0.8, Ti-rich Ca–Ti–O compounds were formed; however, no phases were thermodynamically stable according to the phase diagrams [27, 28]. Under Ca-rich conditions (Ca/Ti supply ratio >1.0), $Ca_{n+1}Ti_nO_{3n+1}$

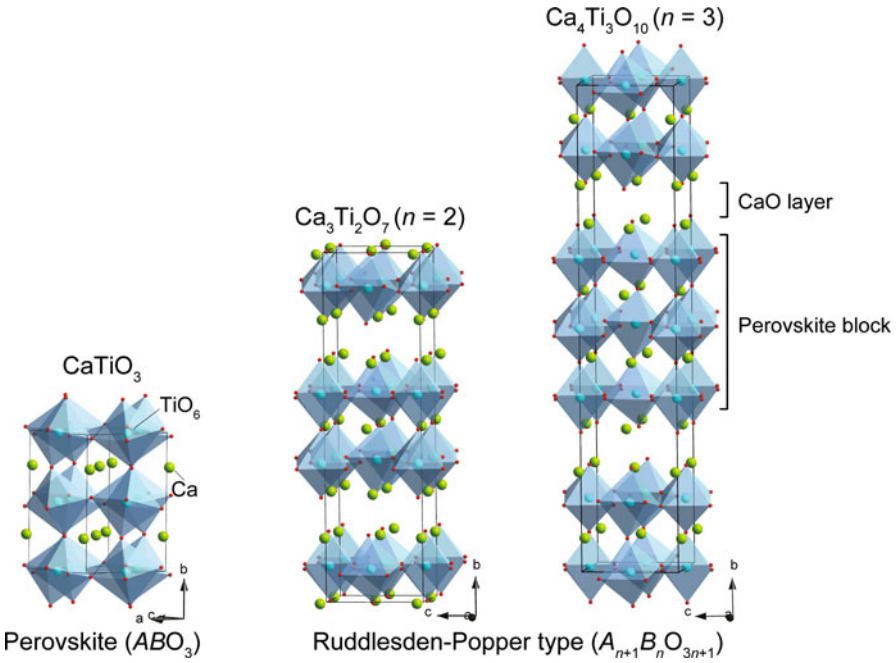

Fig. 4.3 Crystal structures of $CaTiO_3$, $Ca_3Ti_2O_7$, and $Ca_4Ti_3O_{10}$

films were deposited at relatively low deposition temperatures (<1000 K), whereas films prepared at deposition temperatures higher than 1000 K comprised CaO and $CaTiO_3$. In the Ti-rich compositional region between $CaTiO_3$ and TiO_2, several Ca–Ti–O compounds were reported. Bertaut and Blum [32] and Bright et al. [33] reported the synthesis of $CaTi_2O_4$ by electrolysis of TiO_2 and $CaTiO_3$ in a $CaCl_2$ melt. $CaTi_2O_4$ single crystals were synthesized by a flux method from $CaTiO_3$ in $CaCl_2$ and Ti metal [34]. The existence of $CaTi_4O_9$ and $CaTi_2O_5$ was reported in a wet chemical method and sol–gel method [35–38]. Ancora et al. published patents on the production of $CaTi_2O_5$ and $CaTi_5O_{11}$ [39], where the $CaTi_2O_5$ crystal structure differed from that produced by Limar and Kisel [35, 36]. Since these Ti-rich phases were considered to be metastable and decomposed into $CaTiO_3$ and TiO_2 at high temperatures and the synthesis process was limited, the detailed crystal structures and compositions remain unknown. In this study, the X-ray diffraction (XRD) patterns of Ti-rich Ca–Ti–O films by laser CVD in this study were similar to those of $CaTi_2O_5$ and $CaTi_5O_{11}$ reported by Ancora; however, the phase identification was difficult because the films may comprise a mixture of phases and have preferred orientations. The Ti-rich Ca–Ti–O films were transformed into TiO_2 and $CaTiO_3$ by heat treatment (post annealing) at 1273 K. Further investigation of the detailed chemical compositions and microstructure was required for the Ti-rich Ca–Ti–O compounds.

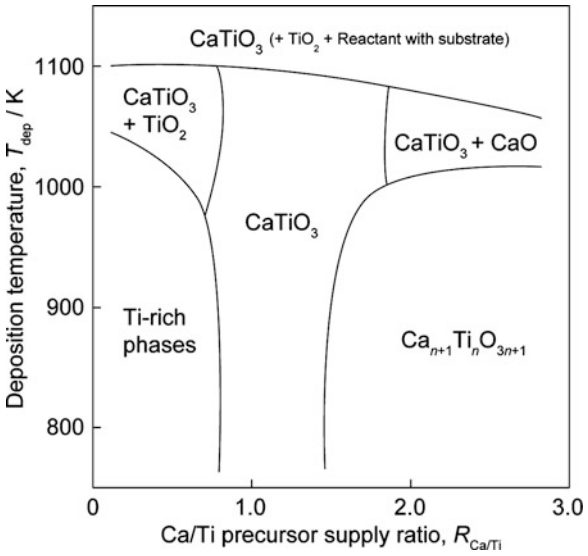

Fig. 4.4 Phase formation relation between deposition temperature and Ca/Ti precursor supply ratio for Ca–Ti–O films formed by laser CVD

Figure 4.5 illustrates the effect of the deposition temperature on the crystal orientations of $CaTiO_3$ films prepared at a total pressure of 800 Pa, where the texture coefficient (*TC*) is the degree of crystal orientation. A *TC* value of 10 corresponds to perfect orientation, whereas a *TC* value of 1 corresponds to random orientation [40]. At temperatures below 800 K, $CaTiO_3$ films with (011) orientation were formed. With an increase in the deposition temperature, the preferred orientation changed from (011) to (101) at approximately 800 K. Further increases in the deposition temperature resulted in the formation of $CaTiO_3$ films having no preferred orientation. The preferred orientation during the growth of $CaTiO_3$ films can be controlled not only by the deposition temperature but also by the total pressure in the chamber. The (121)-oriented $CaTiO_3$ films were deposited in the total pressure range of 400–600 Pa at a deposition temperature of 825–855 K, whereas the preferred orientation was (101) at a total pressure of 800 Pa in the same deposition temperature range (Fig. 4.5). Figure 4.6 shows the typical surface and cross-sectional morphologies of $CaTiO_3$ films with the preferred orientations ((011), (101), and (121)) and without orientation. (011)-oriented $CaTiO_3$ films have a cone-like morphology with pyramidal facets, as shown in Fig. 4.6a. Square facets, which are several micrometers in size, were formed in (101)-oriented $CaTiO_3$ films, as shown in Fig. 4.6c. (121)-oriented $CaTiO_3$ films had a granular morphology with fine grains smaller than several micrometers in size (Fig. 4.6e). These $CaTiO_3$ films with strongly preferred orientations were grown in the columnar regime (Fig. 4.6b, d, f). $CaTiO_3$ films without preferred orientation prepared at a high deposition temperature composed randomly arranged faceted grains (several micrometers in size) with a dense and smooth cross section, as shown in Fig. 4.6c, f.

Figure 4.7 depicts the detailed microstructures with crystal structure models of the corresponding textures in the (011)- and (101)-oriented $CaTiO_3$ films. The

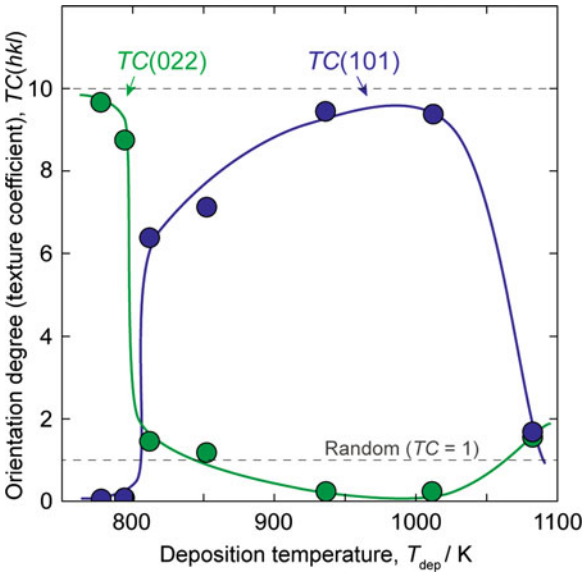

Fig. 4.5 Effect of deposition temperature on *TC*(022) and *TC*(101) of $CaTiO_3$ films

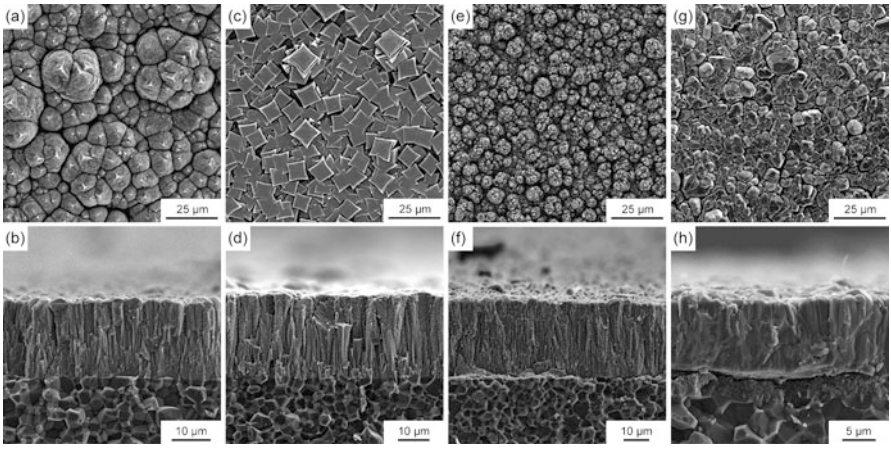

Fig. 4.6 SEM images of typical $CaTiO_3$ films deposited by laser CVD on AlN substrates. (**a**, **b**) (011)-oriented $CaTiO_3$ film at 795 K and 800 Pa, (**c**, **d**) (101)-oriented $CaTiO_3$ film at 935 K and 800 Pa, (**e**, **f**) (121)-oriented $CaTiO_3$ film at 855 K and 400 Pa, and (**g**, **h**) $CaTiO_3$ film with random orientation at 1080 K and 800 Pa

cone-like morphology of the (011)-oriented $CaTiO_3$ film comprised pyramidal facets, which are several tens nanometers in size. Considering the preferred (011) orientation and the shapes of the grains, the pyramidal texture could be associated with the $CaTiO_3$ crystal structure, and the faceted planes would be {010} and {110} as shown in Fig. 4.7b. The microstructure of the square facets in the (101)-oriented $CaTiO_3$ film is shown in Fig. 4.8a. Figure 4.8b shows the terrace on the top surface

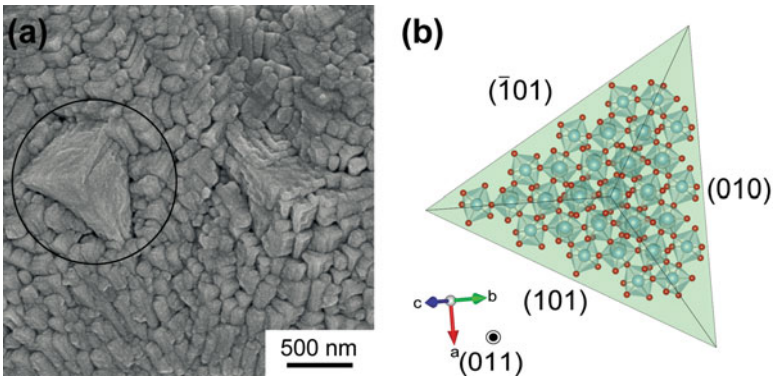

Fig. 4.7 Microstructure and oriented texture of (011)-oriented $CaTiO_3$ film. (**a**) Surface SEM image at high magnification and (**b**) crystallographic texture of the pyramidal facet

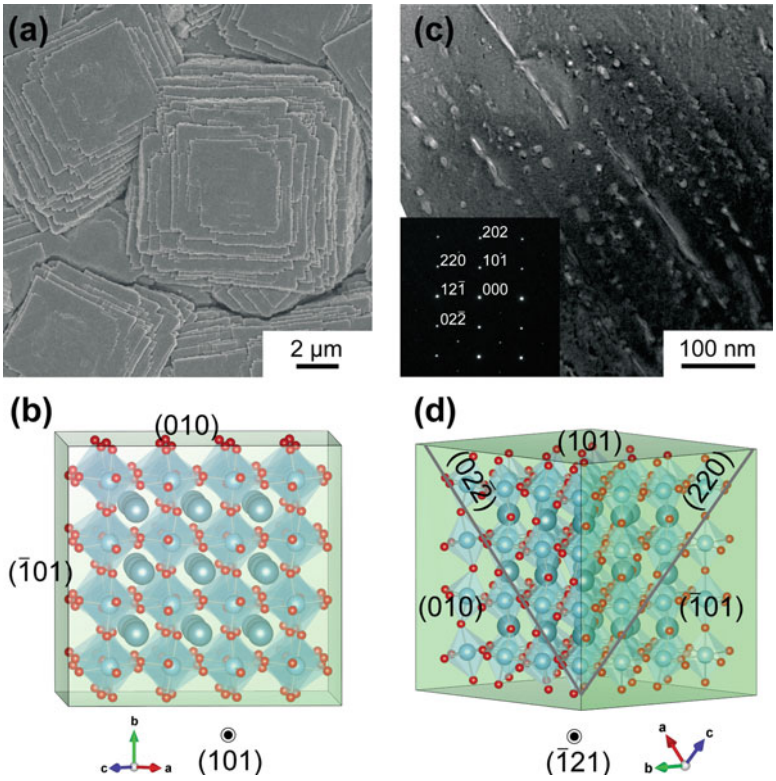

Fig. 4.8 Microstructure and oriented texture of (101)-oriented $CaTiO_3$ film. (**a**) Surface SEM image at high magnification, (**b**) crystallographic texture of the square facet, (**c**) cross-sectional TEM image of the square facet, and (**d**) relation between crystallographic texture and the formation of nanopores

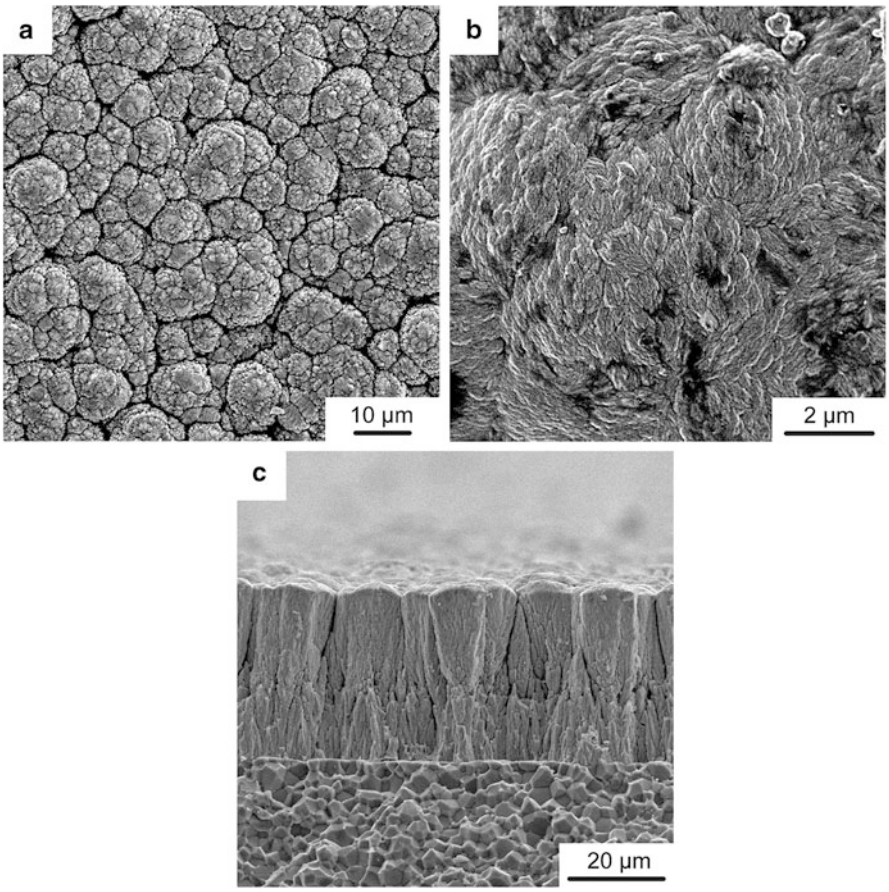

Fig. 4.9 SEM images of a $Ca_nTi_{n+1}O_{3n+1}$ film at 777 K and 800 Pa. (**a**) Surface morphology, (**b**) enlarged image of cauliflower-like grains, and (**c**) cross-sectional image

of the square facet corresponding to the (101) plane, along which the corner-sharing TiO_6 octahedra are aligned. Here, the lateral planes of the square facet were {101} and {010}. In Fig. 4.8c, the cross-sectional transmission electron microscopy (TEM) image of the square facet revealed that nanopores formed along the (110) and (011) planes, which are the close-packed planes of Ca–O atoms. These nanopores may relax the stress between the bio-ceramic films and metallic substrates [41–43].

Figure 4.9 shows the surface and cross-sectional morphologies of the $Ca_{n+1}Ti_nO_{3n+1}$ film prepared at a Ca/Al supply ratio of 1.6 and a deposition temperature of 777 K. The surface exhibited a cone-like morphology with a grain size of approximately 5–10 μm (Fig. 4.10a). Each cone-like grain comprised granules that were several tens nanometers in size. The cross section was cone-like, which is a typical morphology for CVD-deposited films [44]. The Ca/Ti composition of this film was

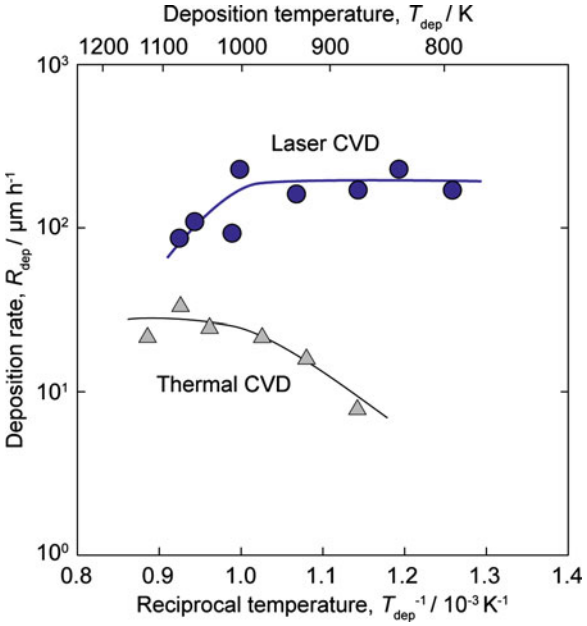

Fig. 4.10 Effect of deposition temperature on deposition rates of $CaTiO_3$ films formed by laser CVD. For comparison, plots of the deposition rates of $CaTiO_3$ films formed by conventional thermal CVD are also included

1.54 by EPMA, which was nearly the same as that of $Ca_3Ti_2O_7$. However, it was difficult to identify the detailed phases in the $Ca_{n+1}Ti_nO_{3n+1}$ films, because the XRD powder pattern of $Ca_3Ti_2O_7$ was similar to that of $Ca_4Ti_3O_{10}$ owing to the same type of long-range perovskite-related structure.

Figure 4.10 shows the temperature dependence of the deposition rate for $CaTiO_3$ films by laser CVD and conventional thermal CVD in an Arrhenius format. The deposition rates of the $CaTiO_3$ films by laser CVD reached 230 μm h^{-1} in the temperature range of 800–1000 K. For the case of conventional thermal CVD, $CaTiO_3$ films without preferred crystal orientation were grown at the deposition rates in the range of 10–30 μm h^{-1} and at deposition temperatures above 900 K. Laser CVD enables the preparation of $CaTiO_3$ with several types of oriented textures at lower deposition temperatures and considerably higher growth rates compared with those obtainable by thermal CVD.

Figure 4.11 depicts the surface morphologies of the $CaTiO_3$ and $Ca_{n+1}Ti_nO_{3n+1}$ films coated on the AlN substrates before and after immersion in SBF (Hanks' solution) for 3 days. Although no significant change in the randomly faceted grains of the $CaTiO_3$ films without preferred orientation occurred during immersion, the grain boundaries and the faceted edges became slightly obscured (Fig. 4.11a, b). On the other hand, for the as-deposited $CaTiO_3$ film comprising square-faceted grains with strong (101) orientation, the edges and corners of the facets became round and smooth after immersion in Hanks' solution (Fig. 4.11c, d). These changes in grain boundaries and facet edges could be caused by the dissolution of $CaTiO_3$ into Hanks' solution, indicating the biosolubility of the $CaTiO_3$ coating. The surface cone-like morphology with pyramidal facets of (011)-oriented $CaTiO_3$ films became

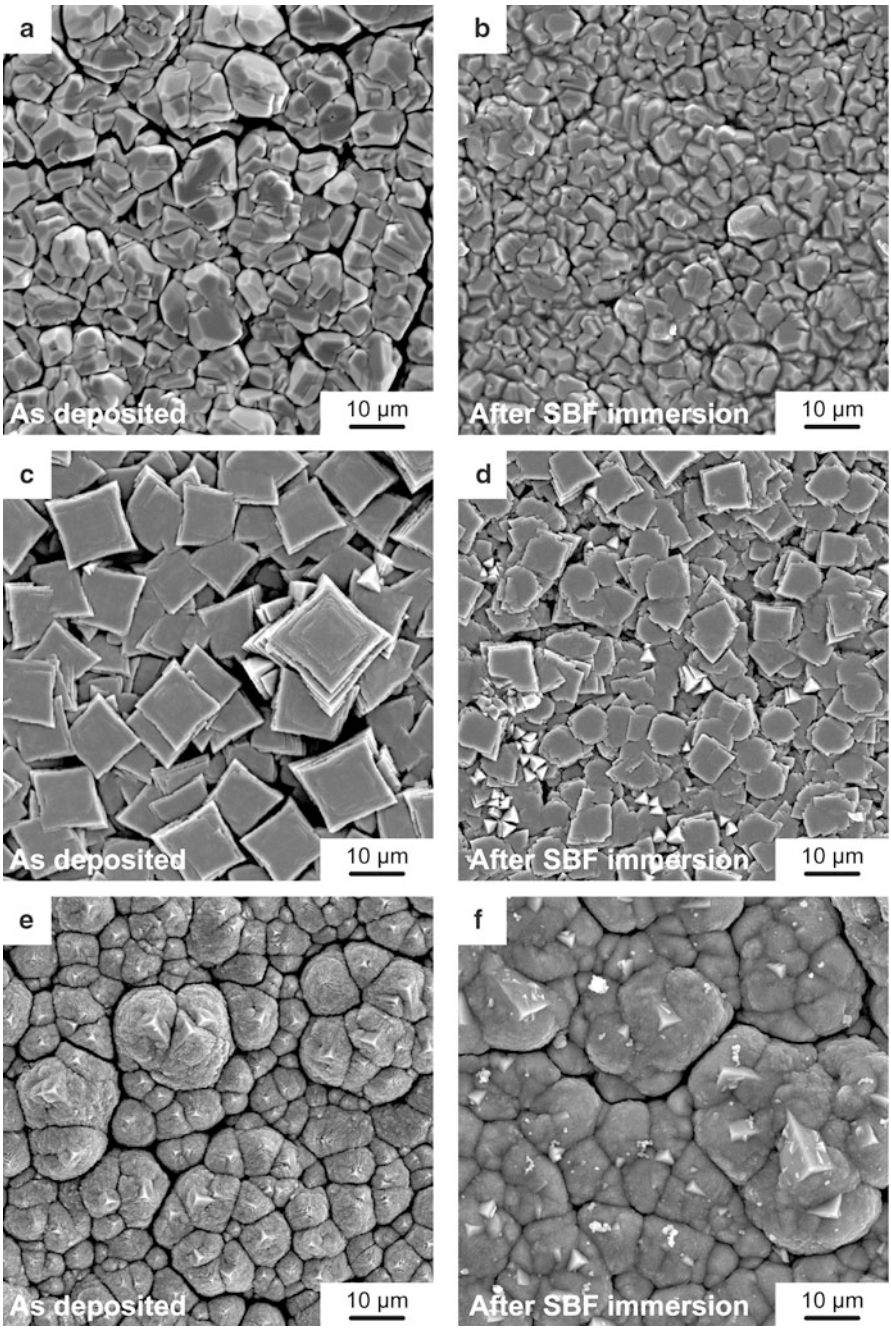

Fig. 4.11 Effect of immersion in Hanks' solution for 3 days on the surface morphologies of $CaTiO_3$ films coated on AlN substrates. (**a**, **b**) $CaTiO_3$ film with random orientation, (**c**, **d**) $CaTiO_3$ film with (101)-orientation, and (**e**, **f**) $CaTiO_3$ film with (011)-orientation. Images (**a**, **c**, and **e)** show as-deposited films, whereas (**b**, **d**, and **f)** show films after the immersion

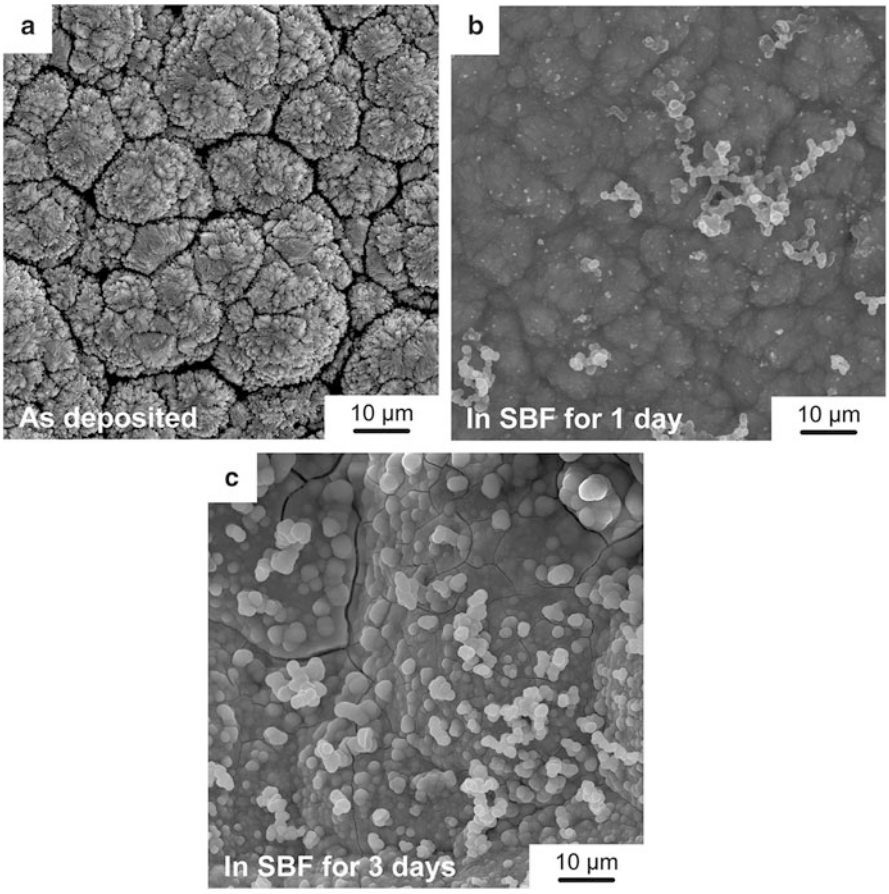

Fig. 4.12 The effect of immersion in Hanks' solution on the surface morphologies of $Ca_nTi_{n+1}O_{3n+1}$ films coated on AlN substrates; (**a**) as-deposited, (**b**) after immersion for 1 day, and (**c**) after immersion for 3 days

smooth, as shown in Fig. 4.11f. Figure 4.11f shows that a small amount of calcium phosphate precipitate (several hundred nanometers in size) with a bright contrast appeared on the film's surface after immersion in Hanks' solution. The biosolubility and calcium phosphate formation of $CaTiO_3$ films are affected by the morphology and preferred orientation. Figure 4.12 depicts the change in the surface morphology of $Ca_{n+1}Ti_nO_{3n+1}$ films caused by immersion in the Hanks' solution. The cauliflower-like grains of the as-deposited $Ca_{n+1}Ti_nO_{3n+1}$ film became smooth, and calcium phosphate precipitate was formed after immersion for 1 day (Fig. 4.12b). The entire surface of the film was covered by calcium phosphate precipitate after 3 days, as shown in Fig. 4.12c. Compared with the conventional perovskite $CaTiO_3$ films (Fig. 4.11), the Ruddlesden–Popper-type $Ca_{n+1}Ti_nO_{3n+1}$ films exhibited significant changes in the surface morphology and high calcium phosphate formation ability after the short-term immersion in SBF.

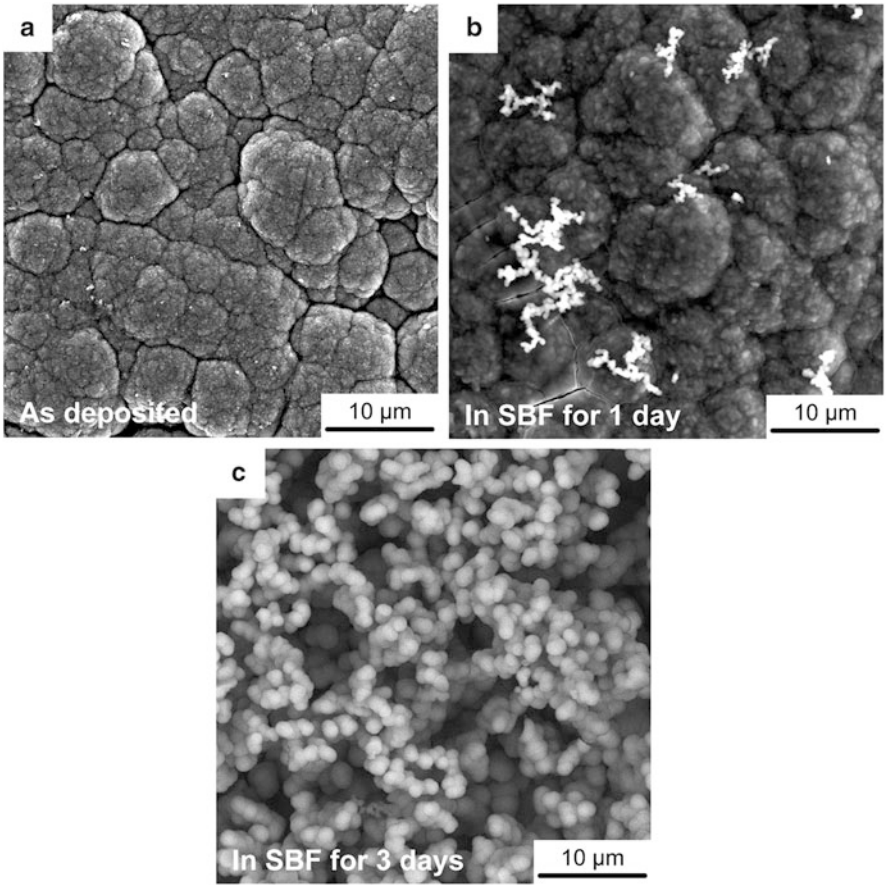

Fig. 4.13 The effect of immersion in Hanks' solution on the surface morphologies of $Ca_nTi_{n+1}O_{3n+1}$ films coated on Ti substrates; (**a**) as-deposited, (**b**) after immersion for 1 day, and (**c**) after immersion for 3 days

$Ca_{n+1}Ti_nO_{3n+1}$ film was coated on a CP-Ti substrate. Figure 4.13 shows the surface morphologies of the $Ca_{n+1}Ti_nO_{3n+1}$ film prepared at a deposition temperature of 620 K on a CP-Ti substrate. The as-deposited $Ca_{n+1}Ti_nO_{3n+1}$ film had a cauliflower-like morphology similar to that on an AlN substrate (Fig. 4.12a). After the SBF immersion for a day (Fig. 4.13b), the surface of the cauliflower-like grains became smooth, and the grain boundaries were obscured. The entire film surface was covered with calcium phosphate precipitate after immersion for 3 days, as shown in Fig. 4.13c. Therefore, laser CVD enables the bio-ceramic coating of $Ca_{n+1}Ti_nO_{3n+1}$ film on Ti substrates, and this coating is promising for enhancing the osteoinductivity of Ti-based implants.

4.4 Summary

Well-crystallized Ca–Ti–O films with various crystal phases and microstructures were produced at high deposition rates by laser CVD. Highly (011)-, (101)-, and (121)-oriented $CaTiO_3$ films were obtained, forming cauliflower-like, granular, and faceted morphologies. These various preferred orientations and morphologies affected the solubility, regeneration of calcium phosphate, and bio-inertness of $CaTiO_3$ films. For the Ca-rich compositions, $Ca_{n+1}Ti_nO_{3n+1}$ films with a Ruddlesden–Popper-type crystal structure were formed and exhibited promising bioactivity for calcium phosphate regeneration.

Acknowledgment This work was supported by the Ministry of Education, Culture, Sports, Science and Technology (MEXT), Scientific Research (A) No. 16H06121 and a cooperative program of the ARCMG-IMR No. 16G0405, Tohoku University.

References

1. Cao H, Liu X. Plasma-sprayed ceramic coatings for osseointegration. Int J Appl Ceram Technol. 2013;10:1–10. doi:10.1111/j.1744-7402.2012.02770.x.
2. Hanawa T. Biofunctionalization of metallic materials: creation of biosis–abiosis intelligent interface. In: Sasaki K, Suzuki O, Takahashi O, editors. Interface oral health science 2014. Tokyo: Springer; 2015. p. 53–64.
3. Hanawa T. Biofunctionalization of titanium for dental implant. Jpn J Dent Sci Rev. 2010;46:93–101. doi:10.1016/j.jdsr.2009.11.001.
4. Ohtsu N, Sato K, Yanagawa A, Saito K, Imai Y, Kohgo T, Yokoyama A, Asami K, Hanawa T. $CaTiO_3$ coating on titanium for biomaterial application—optimum thickness and tissue response. J Biomed Mater Res. 2007;82A:304–15. doi:10.1002/jbm.a.31136.
5. Narushima T. Surface modification for improving biocompatibility of titanium materials with bone. J Jpn Inst Light Metals. 2008;58:577–82. doi:10.2464/jilm.58.577.
6. Ohtsu N, Sato K, Saito K, Asami K, Hanawa T. Calcium phosphates formation on $CaTiO_3$ coated titanium. J Mater Sci Mater Med. 2007;18:1009–16. doi:10.1007/s10856-006-0114-x.
7. Iwasaki M. Fabrication of artificial bone by anodic oxidation of titanium. Surf Finish Soc Jpn. 2014;65:272–5. doi:10.4139/sfj.65.272.
8. Ohtsu N, Sato K, Saito K, Hanawa T, Asami K. Evaluation of degradability of $CaTiO_3$ thin films in simulated body fluids. Mater Trans. 2004;45:1778–81. doi:10.2320/matertrans.45.1778.
9. Rakngarm A, Miyashita Y, Mutoh Y. Formation of hydroxyapatite layer on bioactive Ti and Ti–6Al–4V by simple chemical technique. J Mater Sci Mater Med. 2007;19:1953–61. doi:10.1007/s10856-007-3285-1.
10. Wei D, Zhou Y, Jia D, Wang Y. Formation of $CaTiO_3/TiO_2$ composite coating on titanium alloy for biomedical applications. J Biomed Mater Res. 2008;84B:444–51. doi:10.1002/jbm.b.30890.
11. Ohba Y, Watanabe T, Sakai E, Daimon M. Coating of HAp/$CaTiO_3$ multilayer on titanium substrates by hydrothermal method. J Ceram Soc Jpn. 1999;107:907–12. doi:10.2109/jcersj.107.907.
12. Kačiulis S, Mattogno G, Pandolfi L, Cavalli M, Gnappi G, Montenero A. XPS study of apatite-based coatings prepared by sol-gel technique. Appl Surf Sci. 1999;151:1–5. doi:10.1016/S0169-4332(99)00267-6.

13. Holliday S, Stanishevsky A. Crystallization of $CaTiO_3$ by sol-gel synthesis and rapid thermal processing. Surf Coat Technol. 2004;188–189:741–4. doi:10.1016/j.surfcoat.2004.07.044.
14. Hamada K, Kon M, Hanawa T, Yokoyama K, Miyamoto Y, Asaoka K. Hydrothermal modification of titanium surface in calcium solutions. Biomaterials. 2002;23:2265–72. doi:10.1016/S0142-9612(01)00361-1.
15. Hanawa T, Ukai H, Murakami K. X-ray photoelectron spectroscopy of calcium ion- implanted titanium. J Electron Spectrosc. 1993;63:347–54. doi:10.1016/0368-2048(93)80032-H.
16. Sato M, Tu R, Goto T. Preparation conditions of $CaTiO_3$ film by metal-organic chemical vapor deposition. Mater Trans. 2006;47:1386–90. doi:10.2320/matertrans.47.1386.
17. Goto T. High-speed deposition of zirconia films by laser-induced plasma CVD. Solid State Ion. 2004;172:225–9. doi:10.1016/j.ssi.2004.02.034.
18. Chi C, Katsui H, Tu R, Goto T. Preparation of Na–Al–O films by laser chemical vapor deposition. Mater Chem Phys. 2015;160:456–60. doi:10.1016/j.matchemphys.2015.05.024.
19. Chi C, Katsui H, Goto T. Preparation of Na-beta-alumina films by laser chemical deposition. Surf Coat Technol. 2015;276:534–8. doi:10.1016/j.surfcoat.2015.06.019.
20. Chi C, Katsui H, Tu R, Goto T. Oriented growth and electrical property of $LiAl_5O_8$ film by laser. J Ceram Soc Jpn. 2016;124:111–5. doi:10.2109/jcersj2.15220.
21. Ito A, You Y, Katsui H, Goto T. Growth and microstructure of Ba β-alumina films by laser chemical vapor deposition. J Eur Ceram. 2013;33:2655–6. doi:10.1016/j.jeurceramsoc.2013.04.003.
22. Sato M, Tu R, Goto T. Preparation of hydroxyapatite and calcium phosphate films by MOCVD. Mater Trans. 2007;48:3149–53. doi:10.2320/matertrans.MRA2007145.
23. Sato M, Tu R, Goto T, Ueda K, Narushima T. Hydroxyapatite formation on Ca–P–O coating prepared by MOCVD. Mater Trans. 2008;49:1848–52. doi:10.2320/matertrans.MRA2008097.
24. Goto T, Katsui H. Chemical vapor deposition of Ca–P–O film coating. In: Sasaki K, Suzuki O, Takahashi O, editors. Interface oral health science 2014. Tokyo: Springer; 2015. p. 103–15.
25. Katsui H, Kumagai Y, Goto T. High-speed deposition of highly-oriented calcium titanate film by laser CVD. J Jpn Soc Powder Powder Metall. 2016;63:123–7. doi:10.2497/jjspm.63.123.
26. Katsui H, Kumagai Y, Goto T. High-speed deposition of highly-oriented calcium titanate film by laser CVD. J Jpn Soc Powder Metall. 2016;in press.
27. Kaufman L. Calculation of multicomponent ceramic phase diagrams. Physica B+C. 1988;150:99–114. doi:10.1016/0378-4363(88)90111-8.
28. DeVries RC, Roy R, Osborn EF. Phase equilibria in the system CaO–TiO_2. J Phys Chem. 1954;58:1069–73. doi:10.1021/j150522a005.
29. Sasaki S, Prewitt CT, Bass JD, Schulze WA. Orthorhombic perovskite $CaTiO_3$ and $CdTiO_3$: structure and space group. Acta Cryst. 1987;43:1668–74. doi:10.1107/S0108270187090620.
30. Beznosikov BV, Aleksandrov KS. Perovskite-like crystals of the Ruddlesden-Popper series. Crystallogr Rep. 2000;45:792–8. doi:10.1134/1.1312923.
31. Haenle M, Lindner T, Ellenrieder M, Willfahrt M, Schell H, Mittelmeier W, Bader R. Bony integration of titanium implants with a novel bioactive calcium titanate ($Ca_4Ti_3O_{10}$) surface treatment in a rabbit model. J Biomed Mater Res. 2012;100A:2710–6. doi:10.1002/jbm.a.34186.
32. Bertaut EF, Blum P. Détermination de la Structure de Ti_2CaO_4 par la Méthode Self-Consistante d'Approche Directe. Acta Crystallogr. 1956;9:121–6.
33. Bright NFH, Rowland JF, Wurm JG. The compound CaO.Ti2O3. Can J Chem. 1958;36:492–5. doi:10.1139/v58-070.
34. Rogge MP, Caldwell JH, Ingram DR, Green CE, Geselbracht MJ, Siegrist T. A new synthetic route to pseudo-brookite-type $CaTi_2O_4$. J Solid State Chem. 1998;141:338–42. doi:10.1006/jssc.1998.7932.
35. Limar' TF, Kisel' NG, Cherednichenko IF, Savos'kina AI. Calcium tetratitanate. Russ J Inorg Chem. 1972;17:292–4.
36. Kisel' NG, Limar' TF, Cherednichenko IF. Calcium dititanate. Inorg Mater Transl Izv Akad Nauk SSSR. 8 (1972):1568–70.

37. Pfaff G. Peroxide route to synthesize calcium titanate powders of different composition. J Eur Ceram Soc. 1992;9:293–9. doi:10.1016/0955-2219(92)90064-K.
38. Pfaff G. Synthesis of calcium titanate powders by the sol-gel process. Chem Mater. 1994;6:58–62. doi:10.1021/cm00037a013.
39. Ancora R, Borsa M, Marchi M. Photocatalytic composites containing titanium and limestone. US 2011/0239906 A1. 2011.
40. Rickerby DS, Jones AM, Bellamy BA. X-ray diffraction studies of physically vapour-deposited coatings. Surf Coat Technol. 1989;37:111–37. doi:10.1016/0257-8972(89)90124-2.
41. Kimura T, Goto T. Rapid synthesis of yttria-stabilized zirconia films by laser chemical vapor deposition. Mater Trans. 2003;44:421–4. doi:10.2320/matertrans.44.421.
42. Goto T. Thermal barrier coatings deposited by laser CVD. Surf Coat Technol. 2005;198:367–71. doi:10.1016/j.surfcoat.2004.10.084.
43. Lu TJ, Levi CG, Wadley HNG, Evans AG. Distributed porosity as a control parameter for oxide thermal barriers made by physical vapor deposition. J Am Ceram Soc. 2001;84:2937–46. doi:10.1111/j.1151-2916.2001.tb01118.x.
44. Weiss JR, Diefendorf RJ. Chemically vapor deposited SiC for high temperature and structural applications. Silicon Carbide. Proceedings of the Third International Conference on Silicon Carbide. 1973.